Assurance regions in tracking

D.D. Sworder
Department of ECE
University of California San Diego
dsworder@ucsd.edu

J.E. Boyd
Cubic Defense Systems, Inc.
San Diego, California
john.boyd@cubic.com

R.G. Hutchins
Department of EECE
Naval Postgraduate School
hutchins@nps.navy.mil

R.J. Elliott
Haskayne School of Business
University of Calgary
relliott@ucalgary.ca

Abstract

0403 An assurance region at level p, $\boldsymbol{A}_{\mathcal{P}=p}$, is an area in motion space that contains the target with assigned probability p. It is on the basis of $\boldsymbol{A}_{\mathcal{P}=p}$ that an action is taken or a decision made. Common model-based trackers generate a synthetic distribution function for the kinematic state of the target. Unfortunately, this distribution is very coarse and the resulting $\boldsymbol{A}_{\mathcal{P}=p}$ lack credibility. It is shown that a map-enhanced, multiple model algorithm reduces the tracking error and leads to a compact assurance region.

1 Introduction

Figure 1. Lateral uncertainty is constrained by street width when the target is confined to a road grid.

.

Consider a target moving on the street grid displayed in Figure 1. For the most part, its accelerations are longitudinal with lateral motion restricted by the road width. At a junction, however, the target may (or must) turn: the accelerations are perpendicular to the velocity entering the intersection. Such abrupt, albeit brief, changes in acceleration are difficult to accommodate in a classical linear-Gauss-Markov (LGM) model because the impulsive nature of the acceleration violates the stationarity conventions.

A simple kinematic state for the target, x_t, might consist of a 2D-position vector, χ_t, and a 2D-velocity vector, υ_t. The resulting 4D-LGM kinematics would employ a white acceleration process, $\{w_t\}$, to represent the motion uncertainties—lateral and longitudinal. A model-based tracker generates a putative conditional distribution of the kinematic state, p_t, from which estimates of position and velocity, $\{\hat{\chi}_t\}$ and $\{\hat{\upsilon}_t\}$, flow. In many algorithms; e.g., the EKF, this distribution is Gaussian: $p_t = \mathbf{N}_\zeta(\hat{x}, P_{xx})$. The tracker locates the target at $\hat{\chi}_t$, with an uncertainty determined by $P_{\chi\chi}$.

To illustrate this, consider motion on a road grid shown in the right panel of Figure 2. Beginning at *start* and continuing along the bold path, estimates of location and the computed (1σ)-error ellipse as generated by an EKF are displayed. The tracker does an acceptable job of locating the target. But the error ellipses consistently fail to enclose the true target. This despite the fact that if p_t were true, the median radial tracking error would be only 1.17σ.

In this paper we wish to explore algorithms that generate high fidelity *assurance regions*. An assurance region at level p, $\boldsymbol{A}_{\mathcal{P}=p}$, is a region in path space that contains the target with probability p. It is on the basis of $\boldsymbol{A}_{\mathcal{P}=p}$ that an action is taken or a decision made. For example, suppose the path environment were rich in clutter sources. Tracking would be improved if a gate were placed about the target

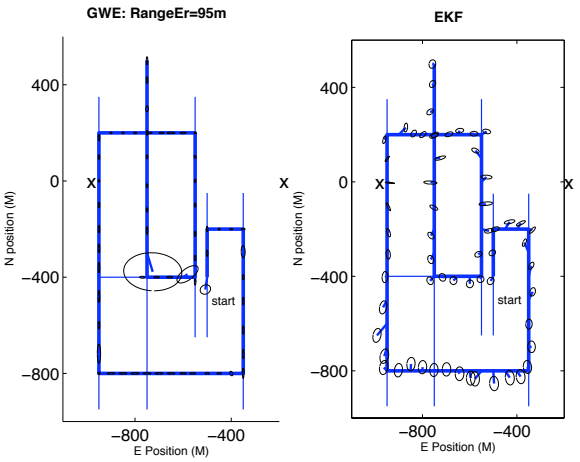

Figure 2. Two trackers follow a vehicle on the indicated road path. There are two position sensors with standard range error 95 m. Shown are the mean-estimates and the (1σ)-error ellipses.

estimate, and only those measurements originating from the gated region were used by the tracker.[1] The area of $\boldsymbol{A}_{\mathcal{P}=p}$ should be as small possible.

Conflict avoidance is another situation in which faithful computation of $\boldsymbol{A}_{\mathcal{P}=p}$ is important. Two targets are not permitted to occupy the same spatial neighborhood. Let the assurance regions of targets one and two be labeled $\boldsymbol{A}_{\mathcal{P}=p}(1)$ and $\boldsymbol{A}_{\mathcal{P}=p}(2)$. Then at level p, an engineer must insist that $\boldsymbol{A}_{\mathcal{P}=p}(1) \cap \boldsymbol{A}_{\mathcal{P}=p}(2) = \phi$. Indeed, the distance between assurance regions is a measure of target separation.

In these illustrations, the size and fidelity of $\boldsymbol{A}_{\mathcal{P}=p}$ is an important adjunct to tracking quality. Unfortunately, the EKF is known to take a rather sanguine view of its own achievements.[2] The accumulation of approximations inherited by p_t is such that its statistics may not be credible. For example, the error ellipses shown in Figure 2 are not representative of the actual error. Delineating $\boldsymbol{A}_{\mathcal{P}=p}$ with $\hat{\chi}$ and $P_{\chi\chi}$ could lead to misfortune.

The EKF is a unimodel algorithm that represents motion uncertainties with a (nearly) isotropic, white acceleration. The factors that distinguish the individual modes on a path composed of segments in the cardinal directions; e.g., speed, velocity, compliance with the junction restrictions, do not enter explicitly into the acceleration model. It is precisely when the motion modes are idiosyncratic that multiple model algorithms become attractive. Instead of a single kinematic template, a family of local models are tuned to the distinctives of the travel mode; e.g., direction, nominal speed.

The tracker studied here is based upon the Gaussian wavelet estimator, GWE. The GWE is a time-discrete hybrid estimator that supervises the simultaneous evolution of a family local filters and associates a state estimate with each. The kinematic disturbance has both structured and unstructured components. The latter is represented by Gaussian white noise. The former, in the role of a random directional process, creates the path seen in the figure. A comprehensive description of the hybrid estimation framework and the GWE is provided in Refs. [3] and [4] and will not be repeated.

The four primitives in the GWE (one for each of the cardinal directions) use the orthodox, time-discrete, CV kinematic representation in the afore mentioned four-dimensional state space with a two-dimensional, white acceleration process.[5]. The primitives are individuated by the eccentricity of their acceleration ellipses. The motion uncertainty is concentrated in the longitudinal direction, with lateral motion tightly constrained by the road width. So, in the N-bound model, the vehicle speed can fluctuate but the direction remains virtually N-bound.

The need for model localization is evident in the N-turn made at the SW-corner of the path shown in the right panel of Figure 2. The estimate of position swings west of the road, and the (1σ)-error ellipses do not capture the actual uncertainty in target position: the error ellipses do not adapt well to changing direction. This is a fundamental limitation on unimodel trackers. Although increased isotropic pseudonoise increases the bandwidth, it also increases the size of the uncertainty regions. This degrades performance on straight path segments and reduces confidence in the estimate. Within a family of models, an engineer can tune the kinematics to the local conditions and accommodate the large accelerations at road junctions.

It is the objective of this paper to demonstrate the performance advantage of a hybrid tracker that integrates map constraints into location estimates. The intent is to achieve the performance shown in the left panel of Figure 2. With two exceptions, the computed (1σ)-error ellipses are so small as to not be visible even though the observations in both panels are the same. The two exceptional points are events of increased ambiguity within the GWE. The error ellipses of the GWE dilate in response to this loss of confidence.

Figures 3 and 4 show the contrasting behaviors of the trackers in more detail. As the target approaches the SW corner from the east, the conditional distribution function for both trackers is (nearly) Gaussian. The figures show a sequence of equi-level contours in position space. The position estimate of the GWE avoids the prohibited region west of -950E. It detects the T-junction at $(-950, -800)$ and correctly turns north—though a south turn is permissible. The equi-level contours generated by the EKF are broad

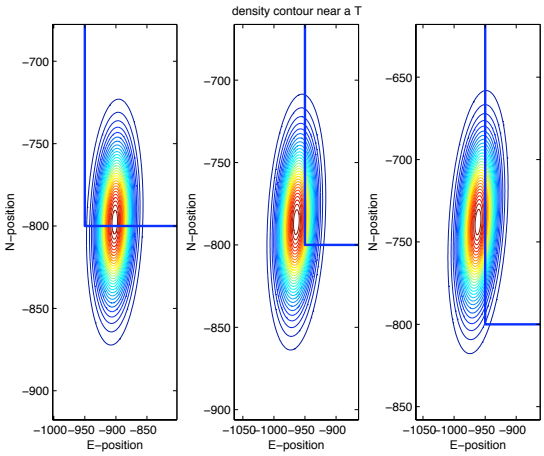

Figure 3. As the west-bound target approaches the SW-road junction, the EKF swings west. Shown are the equi-level contours of the conditional density of position.

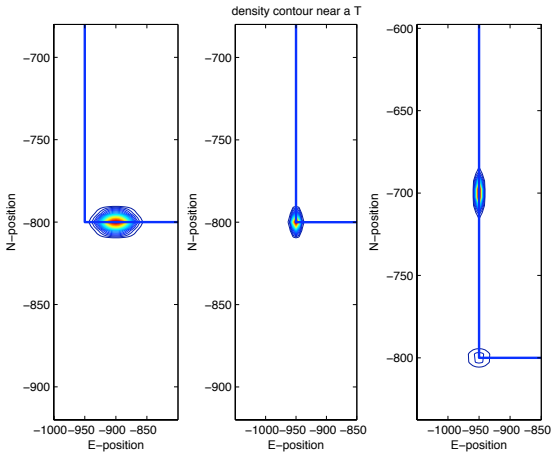

Figure 4. As the west-bound target approaches the SW-road junction, the GWE uses the map to achieve tighter assurance regions.

with a shape corresponding to the sensor geometry. The assurance level following the turn must be increased significantly to capture the true position at at $(-950, -700)$.

The GWE is far superior. The equi-level contours are much tighter than those generated by the EKF. Before the turn, the N-S uncertainty is constrained by road width; the N-S error ellipse in the GWE does not extend 75 m into the prohibited region. The GWE recognizes the T-junction and generates dense and compact confidence regions. Subsequent to the turn, the GWE places the target properly within an eccentric confidence region. The multi-modal nature of p_t is shown by the residual density at the junction in the right panel.

2 Gaussian Wavelet Estimator

The GWE blends several kinematic models, each one associated with a partial path history. Let $\boldsymbol{\iota} \in \kappa$ index the individual filters and let i index the current direction. If the target continues in a specific direction, the target motion is CV with highly eccentric acceleration ellipse: $dv_t = \sqrt{P_i} dw_t$. The major axis of P_i is along the road and the minor axis is small. When the direction changes, position is continuous and the velocity jumps.

The GWE is a predictor-corrector using individuated EKFs that update the current filters and then extend the number of models.

$$(m_{\boldsymbol{\iota}}[k], P_{\boldsymbol{\iota}}[k]) \xrightarrow{\text{EKF}_{\boldsymbol{\iota}}} (m^+_{\boldsymbol{\iota}}[k+1], P^+_{\boldsymbol{\iota}}[k+1]) \quad (1)$$

Gaussian merging is used to maintain a suitable complexity level. The modal-state influence function involves: the kinematic measurements, $y[k+1]$, a speed measurement, $z[k+1]$, of quality, $\mathbf{D}$, and a directional transition rate matrix, Π.

$$\alpha^-_{\boldsymbol{\iota}}[k+1] = \alpha_{\boldsymbol{\iota}}[k] |F^y_{\boldsymbol{\iota}}| \exp \tfrac{1}{2} E^y_{\boldsymbol{\iota}} \quad (2)$$

$$\alpha_{\boldsymbol{\iota}+}[k+1] = \alpha^-_{\boldsymbol{\iota}}[k+1] \Pi_{pi} z[k+1]' \mathbf{D}_{,p} \quad (3)$$

The observation covariances are $\{P^y_{\boldsymbol{\iota}}; \boldsymbol{\iota} \in \kappa\}$, and $E^y_{\boldsymbol{\iota}} = \Delta ||D_{\boldsymbol{\iota}} m_{\boldsymbol{\iota}}||^2_{P^y_{\boldsymbol{\iota}}} - ||y[k+1]||^2_{D^n_{\boldsymbol{\iota}}}$. After renormalization, the one-step smoothed probability of the modal sequence $\boldsymbol{\iota} \in \kappa[k]$, $\{\alpha^+_{\boldsymbol{\iota}}\}$, can be computed. The expanded approximation to the state distribution is: $p[k+1]^- = \sum_{\boldsymbol{\iota} \in \kappa[k]} \alpha^+_{\boldsymbol{\iota}} \mathbf{N}_\zeta (m^+_{\boldsymbol{\iota}}, P^+_{\boldsymbol{\iota}})$.[2]

Although, GWE tunes the directional models, full map fusion was not attempted in the references. To use the map effectively, the junction constraints must be integrated into the extrapolation and measurement update. Specifically, the target vehicle is permitted to turn only at a junction, and the turn must be consistent with the junction type. For example, in the left panel of Figure 2, the W-bound vehicle enters the junction at $(-950, -800)$. It will turn left or right with equal probability. But the vehicle is not permitted to continue west because of topographic constraints.

The GWE avails itself of a ground map, $\mathcal{F}$, that delineates all permissible road segments and junctions. Road segments join individual junctions in the cardinal directions. Each junction is classified according to the permissible ex-

tensions; e.g., a four-way intersection permits all forward directions. The road segments must be compatible with junction location and type.

At a junction, a directional transition rate matrix matched to the junction type suffices for extrapolation. Away from a junction, the direction changes are prohibited. Unfortunately, the GWE does not place the vehicle determinately on $\boldsymbol{F}$. To capture this uncertainty, a blended transition matrix is used in the GWE, smoothly changing as the target approaches a junction. The Mahalanobis distance is useful for quantifying location indeterminacy. After an update, let $\varrho(\hat{x}[k+1])$ be the Mahalanobis distance to the nearest congruent junction. The gauge of the likelihood of encountering the junction during the sample interval used here is $\text{erfc}(0.7\varrho(\hat{x}[k+1]))$.

3 Assurance Regions

To illustrate the construction of an assurance region, consider the motion shown in Figure 2. In this encounter, the roads are better in N-S: the nominal speeds are 20 m/s in N-S and 10 m/s in E-W.There are two range-bearing sensors labeled "$\times$" in the figure. The (1σ)-sensor quality is: 95 m in range 35 mr in bearing (35 m in cross-range at 1 Km). The common measurement interval is 5 seconds. The radar measurements are converted to the common $(X-Y)$-coordinate system and stacked as the vector $y[k]$. Additionally, the sensor suite contains an acoustic, target-speed classifier, $z[k]$, that associates a speed measurement with one of the nominal speeds. The quality is fair: speed is classified correctly 75% of the time.

The continuous motion of the vehicle is sampled to create the time-discrete model. The local models of the GWE are CV. The velocity increment has standard deviation: 0.2 m/s^2 longitudinally and 0.02 m/s^2 laterally in N-S; 0.1 m/s^2 longitudinally and 0.01 m/s^2 in the laterally in E-W.

The EKF is a unitary tracker using a CV model in which the standard deviation of the velocity increment is 0.31 m/s^2 in N-S, and 0.22 m/s^2 the E-W. These accelerations are compatible with the nominal motions but fail to capture the accelerations at turns.

The map, $\boldsymbol{F}$, is used by the GWE for extrapolation and update. Consider the alternatives faced by a W-bound vehicle as it approaches the T-junction at $(-950, -800)$. When far from the junction, the GWE uses the conventional CV-extrapolation to find the forward state estimate, $m_{\iota}^{-}[k+1]$. However, as the vehicle nears the junction, the situation becomes more complex. If $m_{\iota}^{-}[k+1]$ is west of the junction, the vehicle will likely pass through the intersection within the next time sample. But west motion is bounded by the topography. Alternatively, if the forward motion is N-bound, the vehicle must have made the turn at the junction. In this event, the initial state must be reset according to the location

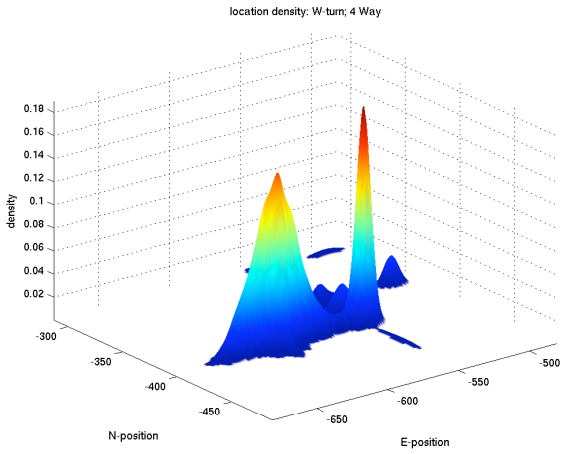

Figure 5. The conditional density past the T-junction, (-550, -400), is multi-modal.

of the junction. There are motion hypotheses that cannot be accommodated within the street grid and extrapolation must be aborted. The modal options are presented in more detail in Ref. [2]. Suffice it to say that modal transition events are useful in correcting location and velocity uncertainty.

With few exceptions, Figure 2 shows the GWE to be so accurate that the error and the error ellipses are not visible on the scale of the figure. There are only two points of significant confusion during the encounter. The $(-550, -400)$ turn is one. As mentioned earlier, this is a T-junction at which the vehicle can continue south, or turn west. The eastward hypothesis is prohibited because the region between -550 E and -500 E is impassible at -400 N.

To see how the GWE views the situation, look carefully at the conditional location density shown in Figure 5. The GWE assigns some probability to the event that the vehicle continues south (permitted) and even some to a north retracing (a U-turn). Most of the probability is found near the true position, $(-600, -400)$, with a narrow lateral spread.

There is also a slender peak at the precedent junction. This incongruity is caused by the rule that aborts the extrapolation for all impermissible motion hypotheses. Probability collects at the last acceptable location; e.g., at the junction. There is even a slight probability that the vehicle is across the forbidden zone at -500 E. This is an artifact of the current GWE logic that updates by placing the estimate at the nearest map location without regard to a violation of topographic constraints.

A map reduces uncertainty in a neighborhood, but ambiguous measurements can make the GWE irresolute. The anomalous point in the left panel Figure 2 near the 4-way intersection at $(-750, -400)$ is a case in point. The west

bound vehicle turns north at this junction. The subsequent (1σ)-error ellipse is quite large as is the location error. For space reasons, the conditional density is not given here. Suffice it to say that the density is multi-modal with significant peaks at nearby (and not so nearby) junctions; e.g., $(-950, -400)$. Note, however, that tracking uncertainty is resolved with the next measurement.

Of interest here is the quality of possible assurance regions generated by the trackers. The tracking error at time $t = kT$ is $\tilde{\chi}[k]$ with covariance $P_{\chi\chi} = D_{\chi\chi}^{-1}$. The standard radial error is $\varrho[\tilde{\chi}[k]] = \sqrt{||\tilde{\chi}[k]||^2_{D_{\chi\chi}}}$. In the LGM problem, the radial error is an iid-sequence of Rayleigh random variables with median equal to 1.17.

As pointed out in Ref. [2], the EKF is an optimistic estimator in that its (1σ)-error ellipses tend to be artificially small. On the path shown, the sample median of $\{\varrho_{ekf}[\tilde{\chi}[k]]\}$ is 4.9; i.e., the median tracking error is four times that predicted by its Gaussian approximation. Consequently, an assurance region generated from $(\hat{x}, P_{xx})$ must use a very large multiple of P_{xx} to assure target inclusion. Unfortunately, a large assurance region creates doubt regarding the validity of the estimate.

The sequence of tracking errors generated by the GWE are neither independent nor Gaussian. Indeed, the median value of $\{\varrho_{gwe}[\tilde{\chi}[k]]\}$ is 0.01. Not only is the radial error much smaller in the GWE tracker, but the standard error has been reduced by 26dB. The mean value of $\{\varrho_{gwe}[\tilde{\chi}[k]]\}$ is considerably bigger than the median; big errors occur near the road junctions. Even using this statistic, the standard error of the GWE is 10dB better than the EKF.

A tight assurance region is achieved by accumulating the points in $p[k]$ with values above a threshold. In the case of the EKF, p_t is Gaussian and $\boldsymbol{A}_{\mathcal{P}=p}$ is simply determined. On straight segments of the path, the conditional density of the GWE is also near Gaussian. The small (1σ)-ellipses produce compact assurance regions. Even the anomalous point after the $(-550, -400)$ west turn shows the GWE to advantage. The lower panel of Figure 6 shows the assurance region, $\boldsymbol{A}^{ekf}_{\mathcal{P}=.92}$. To capture the target on the boundary of $\boldsymbol{A}_{\mathcal{P}=p}$, the inclusion probability had to be widened to $\mathcal{P} = 0.92$.

The upper panel shows the assurance region, $\boldsymbol{A}^{gwe}_{\mathcal{P}=.32}$. To capture the target on the boundary, the inclusion probability had to be only a third of that. The area of $\boldsymbol{A}^{gwe}_{\mathcal{P}=.32}$ is a tenth of $\boldsymbol{A}^{ekf}_{\mathcal{P}=.92}$: $278m^2$ vs. $3970m^2$.

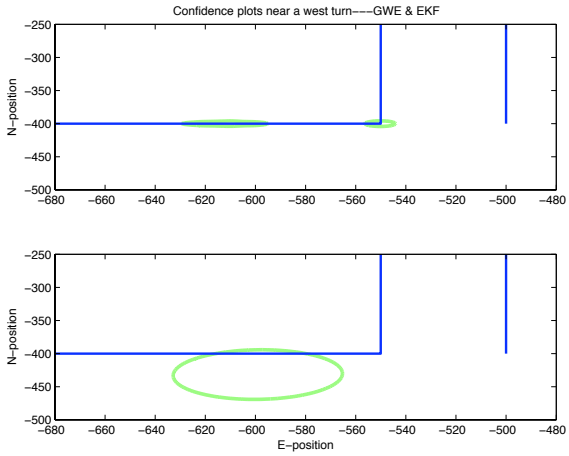

Figure 6. To capture the actual target following the W-turn, the EKF requires an assurance region 14-times bigger.

4 Conclusions

This paper presents assurance regions for two common trackers following a target on a road path. It is shown that $\boldsymbol{A}_{\mathcal{P}=p}$ as computed by the GWE is smaller than that of the EKF: the area of $\boldsymbol{A}^{gwe}_{\mathcal{P}=p}$ is smaller than $\boldsymbol{A}^{ekf}_{\mathcal{P}=p}$ for a given value of p. Additionally, the probability threshold required for $\boldsymbol{A}^{gwe}_{\mathcal{P}=p}$ to include the target is far smaller. An investigation of the properties of $\boldsymbol{A}^{gwe}_{\mathcal{P}=p}$ is ongoing.

References

[1] X. Wang, S. Challa, and R. Evans, "Gating techniques for maneuvering target tracking in clutter," *IEEE Trans. on Aerospace and Electronic Systems* **38**, pp. 1087–1096, July 2002.

[2] D. Sworder, J. Boyd, and R. Hutchins, "Map integration in tracking," *Proc. of the SPIE: Signal and Data Processing of Small Targets* , Aug 2007.

[3] D. Sworder and J. Boyd, *Estimation Problems in Hybrid Systems*, Cambridge University Press, Cambridge, UK, 1999.

[4] D. Sworder and J. Boyd, "Motion models for tracking," *IEEE Trans. on Aerospace and Electronic Systems* **41**, pp. 1052–1056, July 2005.

[5] X. Li and V. Jilkov, "Survey of maneuvering target tracking. part 1: Dynamic models," *IEEE Trans. on Aerospace and Electronic Systems* **39**, pp. 1333–1364, Oct 2003.